Parametric Flutter Analysis of Camber Morphing Wing Using Beam-Plate Coupled Model

Ke Huang, Jiaying Zhang, and Qingyun Wang

Abstract With the development of intelligent materials (including composite material, metamaterial, etc.), advanced actuators (including shape memory alloy, piezoelectric stack, etc.) and other disciplines, the morphing wing can adjust the geometry of the wing adaptively through flexible deformation to ensure the highest aerodynamic efficiency. However, flexible and light wings are prone to induce a structural response by aerodynamic loads, leading to instabilities such as flutter. The main structural modelling approach for conventional flutter problems is to use beam elements or plate elements, which have different accuracy in dealing with different aspect ratios of the wings. Camber morphing wing is mainly composed of the leading edge segment which can't deform and only provides support and the morphing segment which deforms under the drive of actuator. The leading edge is usually treated as a rigid body and only the deformation of the flexible trailing edge is considered in the aeroelastic analysis of the camber morphing wing. For a camber morphing wing with an aspect ratio above 5, the aerodynamic deformation of leading edge structure cannot be ignored due to its large aspect ratio. Since the beam model has two degrees of freedom of deflection and torsion, and the wing deflection is linearly distributed in the chord direction, the beam model will ignore the deformation of the wing in the morphing segment under aerodynamic load, resulting in deviation in the flutter prediction. However, when the high aspect ratio wings are modelled by a rigid-flexible coupled plate model, the flutter prediction is biased due to the limitations of the plate model. For this particular structure, this paper proposes a kind of structure model based on MSC Nastran, which models the leading edge segment using beam elements with relatively large stiffness and the morphing segment using plate elements with small stiffness and combines both parts with rigid bars. The influences of the proportion of the morphing segment, the connection stiffness between the wing and fuselage, and the degree of freedom of fuselage on the flutter characteristics of camber morphing wing are further studied. This will provide a reference for the design of morphing aircraft using passive/active camber morphing wing.

K. Huang · J. Zhang (✉) · Q. Wang
Beihang University, Beijing 100190, China
e-mail: jiaying.zhang@buaa.edu.cn

X. Rui and C. Liu (eds.), *Proceedings of the 2nd International Conference on Mechanical System Dynamics*, Lecture Notes in Mechanical Engineering,
https://doi.org/10.1007/978-981-99-8048-2_113

Keywords Camber morphing wing · Flutter analysis · Beam-plate coupled model

1 Introduction

Morphing aircraft have emerged as a pivotal direction for future aircraft development due to their capability to adaptively adjust their geometry, enabling them to meet diverse mission requirements while maintaining optimal aerodynamic efficiency [1–3]. The progress in smart materials and actuators has driven the design objectives of lightweight aircraft structures for low fuel consumption and high flight performance, leading to the development of morphing wing designs that prioritize flexibility and weight reduction [4]. However, the emphasis on flexibility and lightness in morphing wings introduces the potential risk of aeroelastic instability [5–8].

Currently, the aeroelastic research on traditional wings is quite comprehensive. However, the traditional flutter analysis models based on small deformation assumptions are prone to significant errors when analyzing flexible wings. Therefore, it is necessary to use plate and beam models to accurately describe the flexible deformations of the structure [9]. Modaress et al. [10–12] found that the accuracy of beam and plate models varies when dealing with wings of different aspect ratios. They suggest using plate models for aspect ratios less than 4, and beam models for aspect ratios greater than 4. Gu et al. [13] analyzed the influence of semi-aerodynamic hinges on the aeroelastic characteristics of high aspect ratio wings using beam models and conducted size optimization. Dowell et al. [9, 14–16] summarized the linear and nonlinear flutter characteristics of plate models in subsonic, transonic, and supersonic regimes, and provided the fundamental causes of nonlinear flutter.

Large-scale deformation of flexible wings in morphing aircraft always leads to unsteady aerodynamic characteristics. Both high-precision computational fluid dynamics (CFD) and low-precision potential flow theory are reliable choices [17]. High-precision calculations, however, demand higher model accuracy and greater time costs. Extensive experimental validation has shown that potential flow theory exhibits high accuracy in capturing unsteady lift and flutter characteristics induced by large deformations at subsonic speed, such as waving flags [18, 19], cantilever plates [19–21], and rigid-flexible coupled plate models [22]. Peters et al. [23] proposed a finite-state aerodynamic theory for flexible wings, which was later extended to three-dimensional cases. Walker et al. [24] expanded Theodorsen's unsteady aerodynamic theory, which was initially limited to rigid body motion. Modaress et al. [12] further investigated the combination of Peters' aerodynamic model with plate-beam models, demonstrating significant advantages in computational efficiency and good agreement with experimental data.

Woods and Friswell [25] introduced a novel concept for variable camber wings called Fishbone Active Camber (FishBAC) as shown in Fig. 1. It is a high-performance and structurally simple variable camber wing that enables large and continuous changes in wing camber with minimal actuation energy. Woods and Friswell [26] studied static aeroelasticity using a non-uniform Euler beam

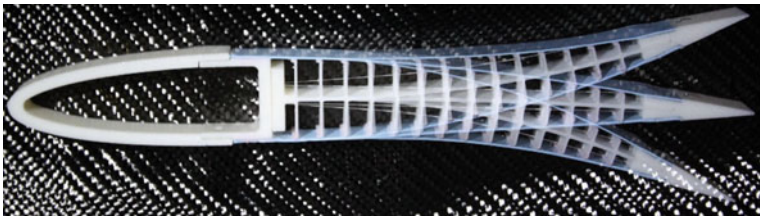

Fig. 1 The structural schematic diagram of FishBAC

model. Rivero et al. [27] investigated the static aeroelastic characteristics of three-dimensional composite flexible wings based on the Mindlin-Love plate model. Zhang et al. [28] developed a rigid-flexible coupled structural model based on FishBAC, representing the flexible segment as a two-dimensional flexible plate under axial flow. Eloy et al. [21] found differences in flutter characteristics between finite-span and infinite-span plates (2D structural model), but currently, there is no research specifically focusing on the flutter characteristics of three-dimensional wings based on FishBAC. Additionally, the influence of aircraft degrees of freedom, elastic boundaries, and flexible segment ratios on wing flutter has not been thoroughly investigated. Therefore, this paper develops a parameterized analysis software using NASTRAN and MATLAB to study the flutter characteristics of FishBAC three-dimensional wings. The effects of degrees of freedom of fuselages, elastic boundaries, and flexible segment ratios on flutter characteristics are examined, providing valuable insights for the design of morphing aircraft in the future.

2 Overview of Morphing Wing Analysis Model

2.1 Problem Analysis and Modeling Method

In reference [28], the authors employed a modeling approach to study the FishBAC two-dimensional cross-segment. They considered the rigid segment as a conventional rigid wing and represented the flexible segment as a Euler beam with significant flexibility. The aeroelastic structural model was established using the Rayleigh–Ritz method and Lagrange's equations. From a three-dimensional perspective, it's reasonable to model the rigid segment of the leading edge as a cantilever beam with an elastic boundary. The flexible segment of the trailing edge is assumed to be connected at one boundary to the rigid leading edge segment and at the other boundary to either the aircraft body or main wing (FishBAC serving as an aileron for traditional wings).

However, traditional beam models often neglect the flexibility of morphing wings' flexible segment under aerodynamic loads, leading to deviations in predicting flutter boundaries and critical damping. It should be noted that there is a substantial stiffness difference between the rigid and flexible segments, typically spanning two orders of

magnitude. Hence, the rigid segment can be effectively modeled as a high aspect ratio cantilever wing, as suggested in [10] for flutter analysis. The flexible plate, being attached to the relatively rigid leading edge segment, can be approximated as a cantilever plate with fixed support at the front end. The aspect ratio of the plate is significantly smaller than 4, thus suitable for a plate model.

Table 1 presents the main parameters of wings studied in this paper, with FishBAC three-dimensional wings having an overall aspect ratio of 5. The structural and aerodynamic models, constructed using MSC Patran, are depicted in Figs. 2 and 3. The model comprises 20 distributed structural elements along the spanwise direction. The number of plate elements is adjusted along the chord direction based on the flexible segment ratio, R_f. Beam elements are modelled by CBAR elements, plate elements by CQUAD4 elements, and rigid connections between the two types of elements are established using RBAR elements. To simulate the elastic boundary, three spring elements (CELAS1) are implemented at the beam's end, including plunge-direction spring K_{UZ}, pitch-direction spring K_{RY}, and rotation-direction spring K_{RX} around the x-axis. Following the modeling approach in references [29, 30], the fuselage is considered a lumped mass (GMASS) connected to the other end of the plunge-direction spring, with the degrees of freedom in the plunge direction released in the constraints to investigate the impact of body degrees of freedom on the flutter characteristics of FishBAC three-dimensional wings.

Table 1 Model parameters of the FishBAC morphing concept

Segment	Parameters	Value	Unit
Total	Chord, c	0.254	m
	Span, L	1.27	m
	Aspect Ratio, AR	5	1
	Fuselage Mass, M_{S}	[0,4]	kg
Rigid segment	Material Modulus, E_{R}	72.0	GPa
	Material Density, ρ_{R}	7200	kg/m^3
	Thickness, t_{R}	2e-3	m
	Elastic axis, x_0	$0.5(1-R_f)\,c$	m
	Pitch stiffness, K_{RY}	[100,2000]	Nm/rad
	Plunge stiffness, K_{UZ}	[100,2000]	N/m
	Stiffness of the spring around the x-axis, K_{RX}	2000	N/m
Morphing segment	Material Modulus, E_{M}	2.14	GPa
	Material Density, ρ_{M}	1040	kg/m^3
	Thickness, t_{M}	2e-3	m
	Flexible segment ratio, R_f	[5,85]	%
Air parameters	Density, ρ_∞	1.226	kg/m^3
	Airspeed, V_∞	(0,150]	m/s
	Mach number, Ma	0	1

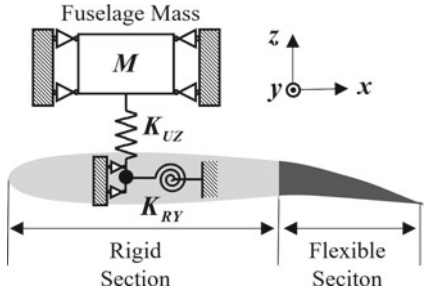

Fig. 2 Wing schematic defining the two segment camber

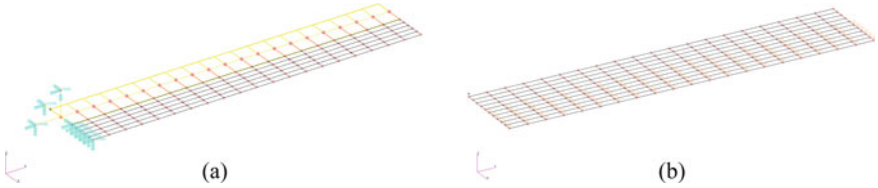

Fig. 3 Aeroelastic model used in the analysis ($R_f = 50\%$) **a** structural model, **b** aerodynamic model

For aerodynamic analysis, the DLM (Doublet-Lattice Method) theory provided by NASTRAN [31] is employed which widely used in conventional aircraft flutter prediction. The beam and plate models are adjusted based on the proportions of the flexible segment, and the interpolation relationship between the structural mesh and the aerodynamic mesh is established using the Infinite Plate Spline method (IPS) and the Infinite Beam Spline method (IBS).

2.2 Program Framework and Implementation

In Table 1, the variables studied in this research are presented as intervals. Consequently, it is necessary to modify the corresponding parameter values in the parametric flutter analysis program. To address various ranges of interest for both structural and computational parameters, a MATLAB text read–write tool is utilized to efficiently generate NASTRAN input files (.bdf) and the associated batch processing files (.bat). Following the completion of computations, the obtained result files (.f06) are processed in bulk to extract key findings, including flutter velocity, flutter frequency, flutter modes, and the natural frequency of the morphing wing. The program framework outlines the procedure for conducting the analysis, as depicted in Fig. 4.

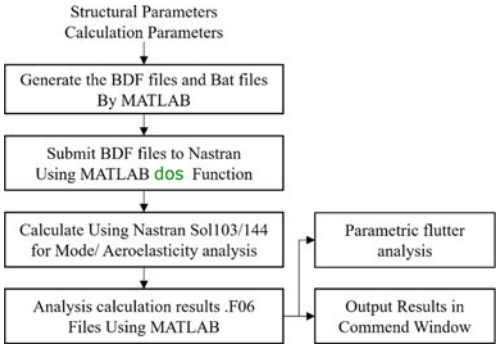

Fig. 4 Program framework established for FishBAC three-dimensional wings

3 Results and Analysis

In this study, a total of 17,508 computational cases were conducted to investigate the influence of two scenarios (with and without body degrees of freedom), 5 parameter points for body mass values ranging from 0 to 4, 13 parameter points for plunge and pitch stiffness values ranging from 100 to 2000, and 17 parameter points for flexible segment ratios ranging from 5 to 85%. The analysis aimed to examine the effects of body degrees of freedom, mass of fuselage, elastic boundary conditions, and flexible segment ratios on the flutter characteristics. Due to space limitations and a large number of computational cases, this paper only analyzes the results of a few selected cases with typical characteristics.

3.1 Theoretical Analysis

According to reference [32], the inclusion of body degrees of freedom can lead to the occurrence of body freedom flutter (BFF) prior to the conventional bending-torsion flutter and static aeroelastic divergence. Therefore, this paper investigates the influence of body degrees of freedom on the flutter boundary of morphing aircrafts. Due to the complex flutter mechanisms of morphing wings, there exist not only the traditional bending-torsion flutter found in conventional flutter analysis but also potential flutter issues associated with flexible segments resembling control surfaces flutter which need to be avoided to ensure controllability of aircrafts. Additionally, the presence of body degrees of freedom can trigger flutter in the rigid-body modes, known as body freedom flutter or dynamic divergence.

To illustrate body freedom flutter in a vivid manner, readers can conceptualize it as a simple harmonic vibration of foundation in the plunge direction. Similar to bending-torsion flutter, body freedom flutter is coursed by the plunge motion of the rigid body and the pitch motion of the wing. As the flight speed increases, there exists a critical phase angle difference between the plunge motion and the pitch motion. This leads to a situation where the unsteady aerodynamic work done exceeds

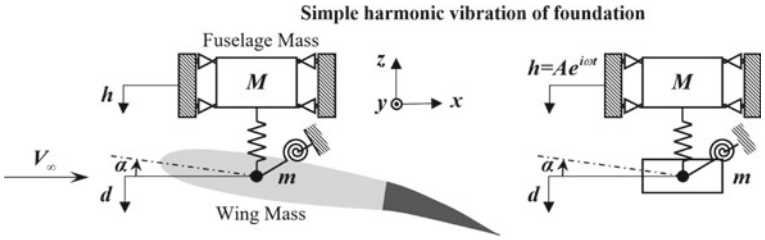

Fig. 5 Diagram of simple harmonic vibration of foundation

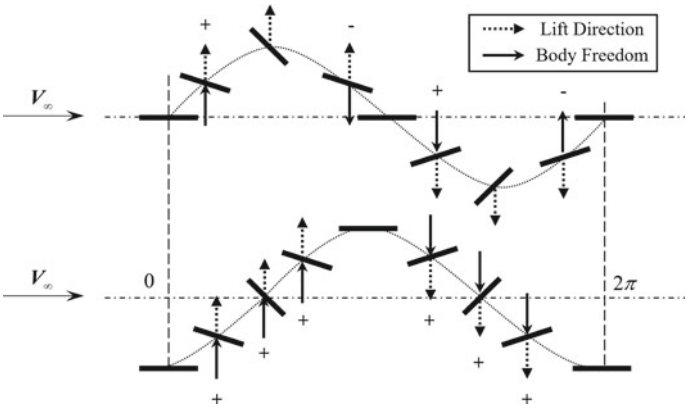

Fig. 6 Energy balance of wing in coupling of body and pitch freedom

the damping dissipated, resulting in a dynamic aeroelastic instability. Schematic diagrams depicting this phenomenon are shown in Figs. 5 and 6. In this study, the focus is not on categorizing the types of flutter but rather on investigating the influence of structural parameters on the flutter boundary. Therefore, all dynamic aeroelastic instability of all degrees of freedom are collectively referred to as flutter.

3.2 Influence of Flexible Segment Ratio

To investigate the influence of the flexible segment ratio on the flutter characteristics of the wing, a body mass of 2 kg was chosen as the cruising payload for analysis in this section with the consideration of wing dimensions and typical cruising conditions. As shown in Fig. 7, the trends of various structural parameters with respect to the flexible segment ratio are depicted. Figure 7a shows the variations of the wing's center of mass and elastic axis as the deformation segments change, while Fig. 7b illustrates the changes in the generalized masses of the two degrees of freedom of the wing with respect to the deformation segments. It can be observed that the position

of the structural elastic axis decreases linearly from 50 to 0% as the flexible segment ratio changes, and the consideration of fuselage mass significantly alters the inertia characteristics, especially in relation to the distance between the elastic axis and the center of mass. Figure 7c and d represent the analysis variables in the simplified two-degree-of-freedom model analyzed in the literature [32]. Figure 7c shows the ratio of uncoupled plunge natural frequency ω_d to uncoupled pitch natural frequency ω_α, which exhibits a trend of increasing and then decreasing with the change in the flexible segment ratio, reaching its maximum at 60%. Figure 7d presents the dimensionless rotational radius and dimensionless static unbalance parameter. It can be observed that the consideration of fuselage mass has a significant impact on these two parameters, which is similar to the trends observed in Fig. 7a and b, and further elaboration is not provided in this context.

As shown in Fig. 8, the contour plots illustrate the variations of flutter velocity and flutter frequency of the system with respect to the flexible segment ratio and K_{RY}. Specifically, for the investigated morphing wing in this study, within the range of 0

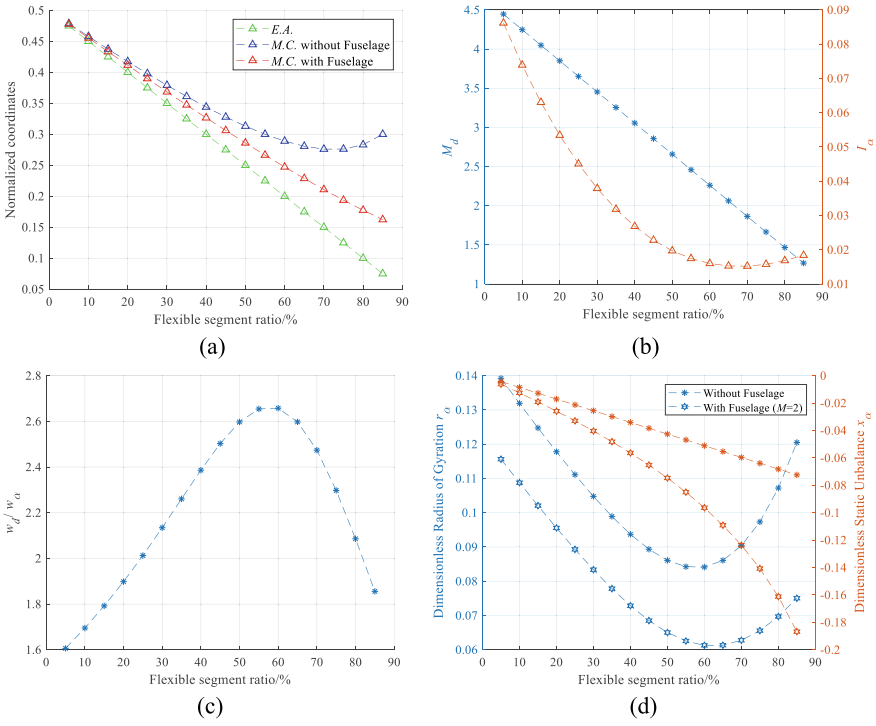

Fig. 7 Diagram of structural parameters and flexible segment ratio. **a** Elastic axis position and center of mass position (with fuselage and without fuselage). **b** Generalized mass of plunge d and pitch freedom α ($E.A.$ = elastic axis, $M.C.$ = central of mass). **c** Ratio of uncoupled plunge natural frequency ω_{d} to pitch natural frequency ω_{α}. **d** Dimensionless parameters for different flexible segment ratios

N/m $\leq K_{UZ} \leq$ 600 N/m, the flutter velocity exhibits an increasing-then-decreasing trend, reaching its maximum at a flexible segment ratio of 60%. On the other hand, the maximum flutter frequency is primarily concentrated at 15%, and it continuously increases with larger K_{UZ} values. In the range of 700 N/m $\leq K_{UZ} \leq$ 2000 N/m, the trend of flutter velocity remains consistent, but the maximum flutter frequency decreases, with peak values occurring at 15% and 50% locations. Figure 8a illustrates the case of $K_{UZ} = 100$ N/m, where the flutter velocity varies from 25.8 to 38.1 m/s with changing flexible segment ratio, reaching its maximum at a ratio of 60%. The corresponding flutter frequency varies from 2.46 to 4.51 Hz. To simplify the analysis, this study refers to the findings in reference [32] regarding simplified two-degree-of-freedom wings to explain the observed phenomena in Fig. 8. Specifically, when the ratio of the uncoupled plunge natural frequency to the pitch natural frequency is greater than 1.5, a monotonic increase in flutter velocity with respect to the frequency ratio is observed. Figure 7c shows that the system's ratio of uncoupled plunge natural frequency to pitch natural frequency exhibits a similar increasing-then-decreasing trend with the flexible segment ratio, reaching its maximum at a ratio of 60%. The literature also indicates that increasing the dimensionless static unbalance x_α and decreasing the dimensionless radius of gyration r_α will reduce the flutter velocity. However, the frequency ratio has a greater impact on the flutter velocity and is considered the primary factor influencing the critical flutter velocity of the system. The flutter frequency exhibits a more complex pattern, which can be attributed to the changes in flutter modes. A detailed analysis of this phenomenon is provided in Sect. 3.4.

3.3 Influence of Body Freedom and Mass of Fuselage

Based on the analysis in Sect. 3.1, it was found that the presence of body freedom is often overlooked in traditional flutter analysis. This is primarily due to the large stiffness of conventional aircraft, where the natural frequency of the rigid body freedom is much smaller than the structural natural frequencies. However, for morphing aircraft, there is often a strong aerodynamic coupling between the rigid body motion and the wing's elastic motion [33], making this issue non-negligible.

As shown in Fig. 9, considering the body freedom and neglecting it yield different phenomena. Considering the body freedom leads to a decrease in the critical flutter velocity, and as the aircraft mass varies, the decrease in the critical flutter velocity becomes more pronounced. As shown in Fig. 9a, when the flexible segment ratio is 60%, the flutter velocities for mass variations from 0 to 4 kg are 40.7 m/s, 40.4 m/s, 39.2 m/s, 36.2 m/s, and 31.1 m/s, respectively. In contrast, the flutter velocity for a body without degrees of freedom is 41.6 m/s. According to the conclusions in reference [32] and the results in Fig. 7d, considering the body degrees of freedom indicates that an increase in mass leads to an increase in x_α and a decrease-then-increase trend in r_α as the flexible segment ratio changes. The increase in x_α and decrease in r_α result in a reduction in flutter velocity. Based on existing theories,

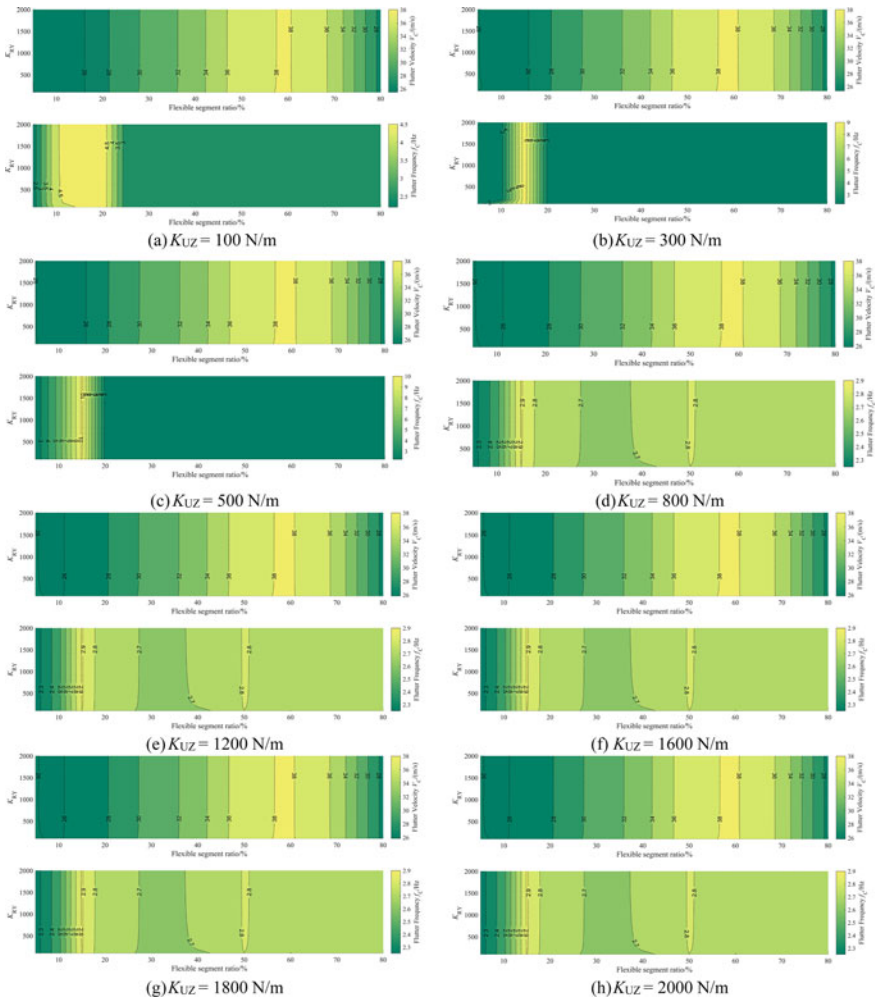

Fig. 8 Flutter speed and frequency for different ratios of flexible segment ratio (%)

the impact of r_α on flutter velocity is greater, showing an overall decreasing trend. Moreover, as the mass increases, the aircraft is more prone to experiencing flutter (Figs. 10 and 11).

3.4 Influence of Boundary Connection Stiffness

As shown in Fig. 12, it illustrates the influence of the stiffness of the elastic boundary on the flutter velocity, flutter frequency, and mode numbers for different flexible

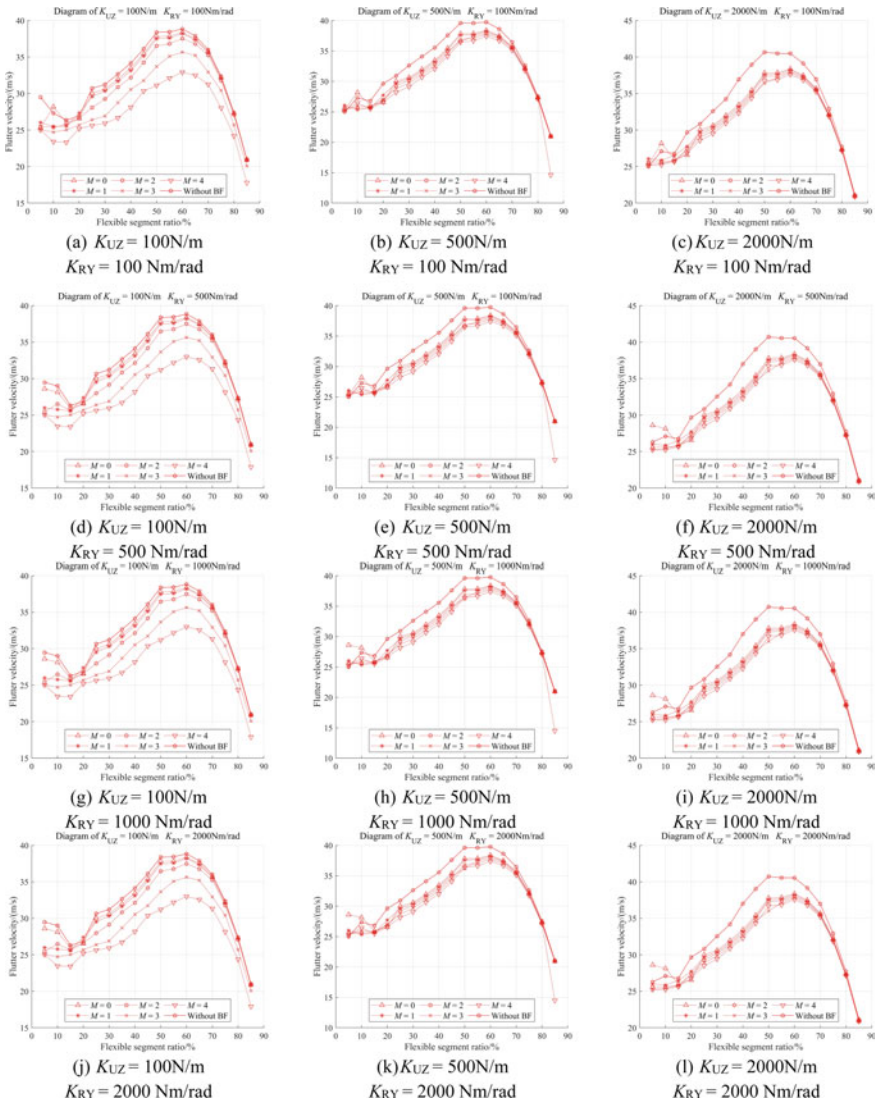

Fig. 9 Comparison of restrained and unrestrained vehicles with different fuselage mass

segment ratios. The effect of the stiffness of boundary connection on the system is rather complex. However, upon careful observation of all the computed results, a conclusion can be drawn that the pitch stiffness has a higher impact on the flutter characteristics of the system compared to the plunge stiffness. Additionally, variations in the plunge stiffness often lead to a minor decrease or an initial increase followed by a decrease in the flutter velocity. This is because an increase in plunge

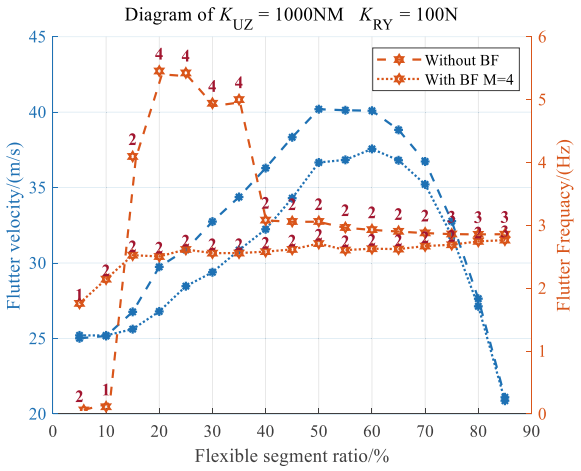

Fig. 10 Comparison of restrained and unrestrained vehicles ($M = 4$)

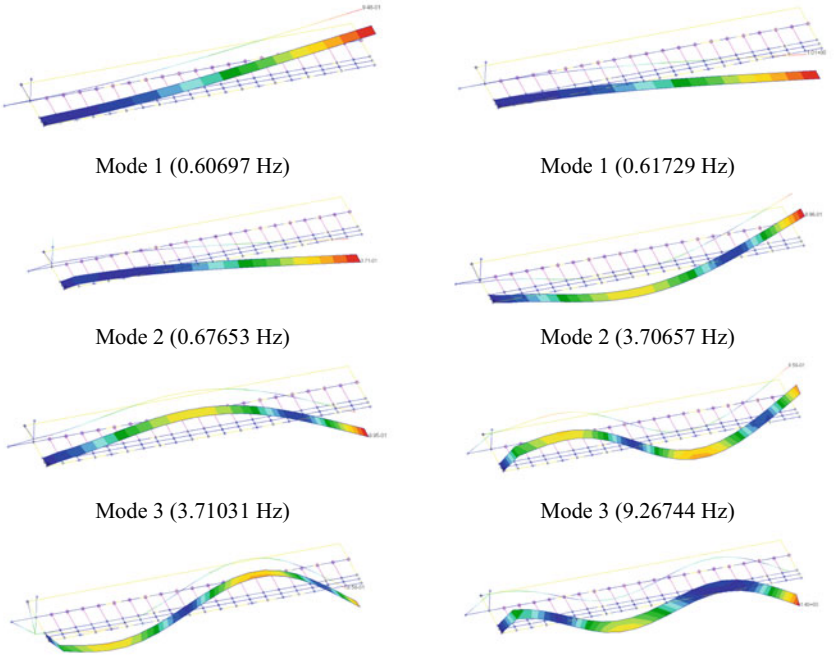

Mode 1 (0.60697 Hz) Mode 1 (0.61729 Hz)

Mode 2 (0.67653 Hz) Mode 2 (3.70657 Hz)

Mode 3 (3.71031 Hz) Mode 3 (9.26744 Hz)

Mode 4 (9.27308 Hz) Mode 4 (15.1416 Hz)

(a) With body freedom ($M = 4$) (b) Without body freedom

Fig. 11 Natural modes and frequencies of the first four order structures ($R_f = 20\%$)

stiffness results in a greater transfer of aerodynamic work to the pitch degree of freedom, leading to a decrease in flutter velocity.

Due to the large volume of computational data, only two typical characteristics of the computed results are summarized as follows:

(1) With variations in stiffness, the flutter velocity and flutter frequency exhibit smooth and continuous changes, with lower flutter velocities associated with smaller torsional stiffness.
(2) With variations in stiffness, there are local discontinuous changes and abrupt transitions in the flutter velocity and flutter frequency, primarily occurring in the variations of torsional stiffness, while the influence of pitch stiffness is relatively small.

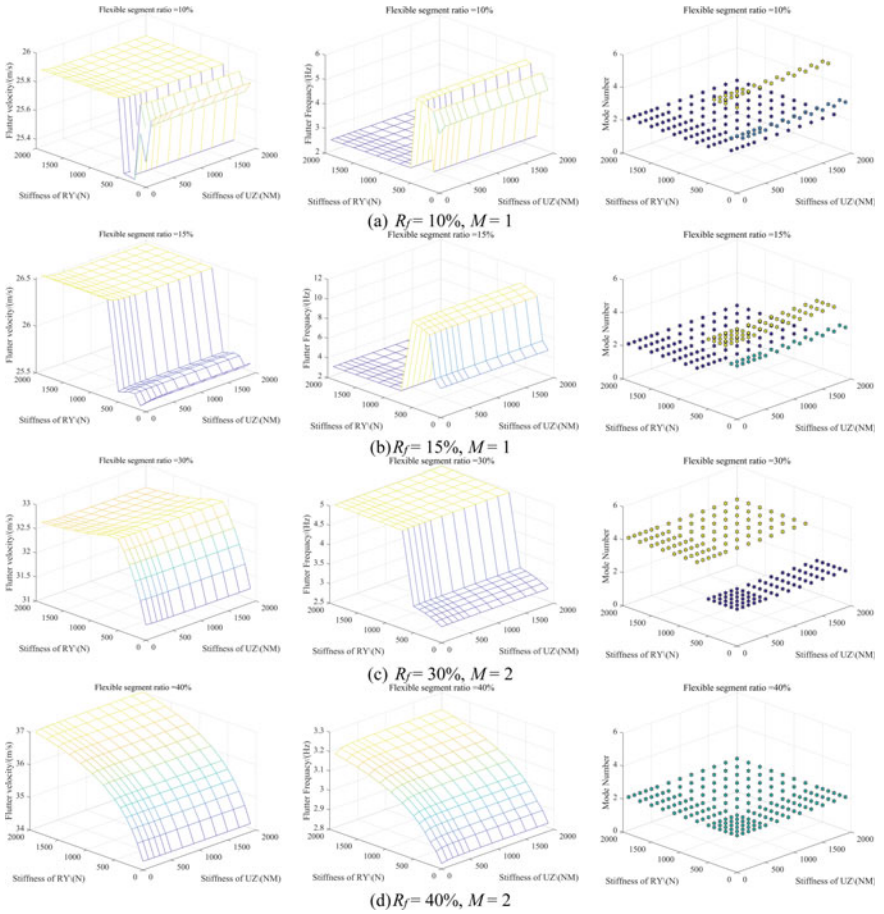

Fig. 12 Flutter speed, frequency and mode number for different boundary connection stiffness

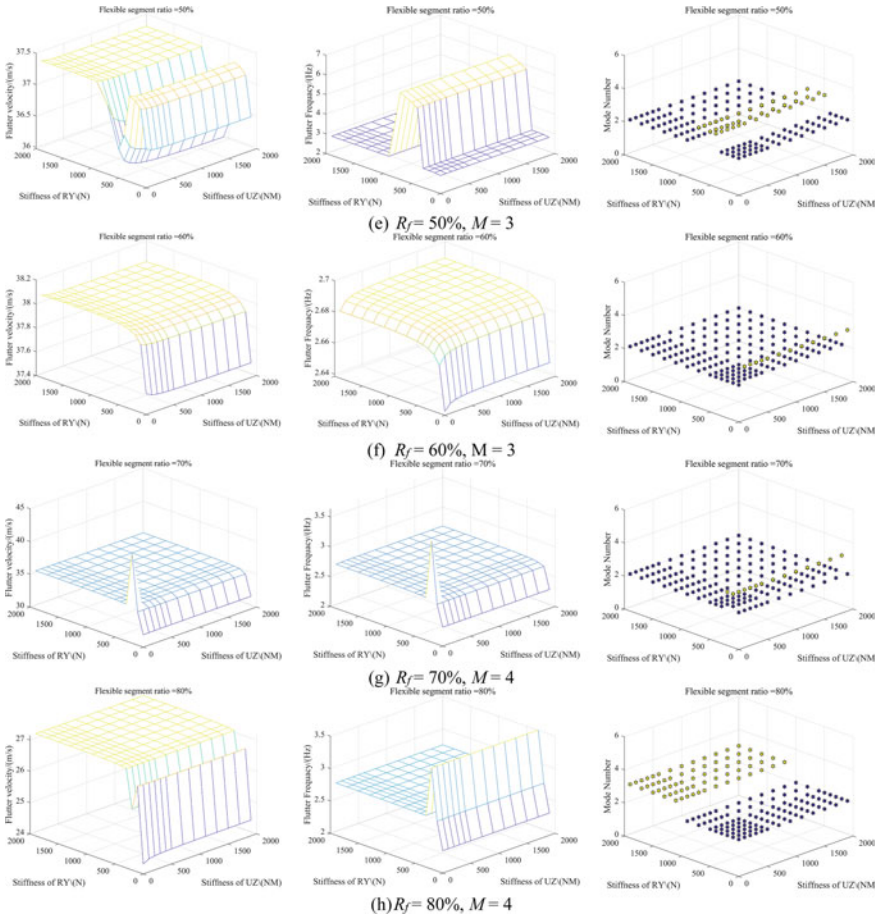

Fig. 12 (continued)

It can be observed that the main difference lies in whether there is an abrupt transition in the flutter velocity, and whenever such a transition occurs, there is a corresponding abrupt change in the flutter frequency. Furthermore, considering the flutter modes that occur, it can be deduced that all the transitions are accompanied by a change in the mode numbers associated with flutter velocity. This is consistent with the conclusion in Sect. 3.1 that various factors contributing to flutter are coupled with each other.

As depicted in Fig. 12a and b, three flutter modes occur within the range of stiffness variations, corresponding to multiple abrupt changes in flutter velocity and frequency. Particularly in Fig. 12a, with four mode transitions, the flutter frequency exhibits significant fluctuations. Similarly, in Fig. 12c, e-h, two flutter modes emerge within the range of stiffness variations, resulting in corresponding changes in flutter frequency. In Fig. 12e, after a mode transition from the 2nd mode to the 3rd mode,

the flutter mode reverts back to the 2nd mode as the stiffness changes. Figure 12d shows only one flutter mode, and it can be observed that its surface is smooth. Since there are no mode transitions, the variation in flutter frequency is not substantial. These abrupt changes in flutter characteristics caused by mode transitions need to be highly considered during the design process of morphing aircraft. In the operational phase of a morphing aircraft, variations in connection stiffness may occur due to fatigue aging or loosening of screws, leading to abrupt changes in flutter velocity. Taking Fig. 12h as an example, if the torsional stiffness is designed to be 1000 N/m, the corresponding flutter velocity is 27.4 m/s. However, if the torsional stiffness decreases to 100 N/m, the flutter velocity will decrease to 24.1 m/s, representing a nearly 12% reduction in flutter velocity. This situation can potentially pose safety risks to the aircraft's operation.

4 Concluding Remarks

In this study, a parameterized analysis program for variable camber wings, developed using NASTRAN and MATLAB, is utilized to investigate the influence of flexible segment ratio, body freedom, fuselage mass, and boundary connection stiffness on the flutter characteristics of morphing aircraft. The obtained results provide valuable references for the subsequent design of morphing aircraft. The following conclusions were drawn:

(1) Considering the body freedom significantly alters the flutter boundary of the aircraft. For the adaptive variable camber wings examined in this study, it was found that considering body freedom reduces the flutter boundary, with a greater reduction observed as the body mass increases. This presents new requirements for loads of morphing aircrafts.
(2) Among the variations in stiffness, the pitch stiffness has a greater impact on the flutter boundary of the aircraft compared to the plunge stiffness. Furthermore, variations in pitch stiffness may lead to abrupt transitions in flutter modes. When considering high flutter velocities as the design criterion, a decrease in connection stiffness may result in an abrupt transition to lower flutter velocities. This highlights new concerns for the design and maintenance of morphing aircraft.
(3) Taking into account both control efficiency and flutter boundary, flexible segment ratio of 60% is a prudent choice. Increasing the flexible segment ratio also reduces the pitch stiffness and mass of the structural rigid segment, but it may pose a risk of lowering the flutter boundary.

Acknowledgements The authors gratefully acknowledge the funding of the National Natural Science Foundation of China (grant number 12102017, 92271104) and the Fundamental Research Funds for the Central Universities (grant number YWF-22-L-1210).

References

1. Barbarino S, Bilgen O, Ajaj RM et al (2011) A review of morphing aircraft. J Intell Mater Syst Struct 22(8):823–877
2. Shi R, Wan W (2015) Analysis of flight dynamics for large-scale morphing aircraft. Aircraft Eng Aerosp Technol: Int J 87:38–44
3. Beaverstock CS, Fincham J, Friswell MI, Ajaj RM et al (2014) Effect of symmetric & asymmetric span morphing on flight dynamics. In: AIAA atmospheric flight mechanics conference, Reston, Virginia
4. Isukapalli SS (1999) Uncertainty analysis of transport-transformation models. Rutgers The State University of New Jersey, School of Graduate Studies
5. Ajaj RM, Parancheerivilakkathil MS, Amoozgar M et al (2021) Recent developments in the aeroelasticity of morphing aircraft. Prog Aerosp Sci 120:100682
6. Chai Y, Gao W, Ankay B et al (2021) Aeroelastic analysis and flutter control of wings and panels: a review. Int J Mech Syst Dyn 1(1):5–34
7. Li D, Zhao S, Da Ronch A et al (2018) A review of modelling and analysis of morphing wings. Prog Aerosp Sci 100:46–62
8. Tiomkin S, Raveh DE (2021) A review of membrane-wing aeroelasticity. Prog Aerosp Sci 126:100738
9. Dowell EH (1974) Aeroelasticity of plates and shells. Springer Science & Business Media
10. Modaress-Aval AH, Bakhtiari-Nejad F, Dowell EH et al (2023) Comparative study of beam and plate theories for moderate aspect ratio wings. AIAA J 61(2):859–874
11. Modaress-Aval AH, Bakhtiari-Nejad F, Dowell EH et al (2020) Aeroelastic analysis of cantilever plates using Peters' aerodynamic model, and the influence of choosing beam or plate theories as the structural model. J Fluids Struct 96:103010
12. Modaress-Aval AH, Bakhtiari-Nejad F, Dowell EH et al (2019) A comparative study of nonlinear aeroelastic models for high aspect ratio wings. J Fluids Struct 85:249–274
13. Gu H, Healy F, Rezgui D et al (2023) Sizing of high-aspect-ratio wings with folding wing-tips. J Aircr 60(2):461–475
14. Dowell EH (1966) Nonlinear oscillations of a fluttering plate. AIAA J 4(7):1267–1275
15. Dowell EH (1967) Nonlinear oscillations of a fluttering plate. II. AIAA J 5(10):1856–1862
16. Dowell EH (2015) Nonlinear aeroelasticity. A modern course in aeroelasticity: Fifth Revised and Enlarged Edition, pp 487–529
17. Anderson J (2011) Fundamentals of aerodynamics. McGraw-Hill
18. Taneda S (1968) Waving motions of flags. J Phys Soc Jpn 24(2):392–401
19. Argentina M, Mahadevan L (2005) Fluid-flow-induced flutter of a flag. Proc Natl Acad Sci 102(6):1829–1834
20. Tang DM, Yamamoto H, Dowell EH (2003) Flutter and limit cycle oscillations of two-dimensional panels in three-dimensional axial flow. J Fluids Struct 17(2):225–242
21. Eloy C, Souilliez C, Schouveiler L (2007) Flutter of a rectangular plate. J Fluids Struct 23(6):904–919
22. De Breuker R, Abdalla MM, Gurdal Z (2008) Flutter of partially rigid cantilevered two-dimensional plates in axial flow. AIAA J 46(4):936–946
23. Peters DA, Hsieh MCA, Torrero A (2007) A state-space airloads theory for flexible airfoils. J Am Helicopter Soc 52(4):329–342
24. Walker WP, Patil MJ (2014) Unsteady aerodynamics of deformable thin airfoils. J Aircr 51(6):1673–1680
25. Woods BKS, Friswell MI (2013) Structural analysis of the fish bone active camber concept. In: Conference 2013, vol 912
26. Woods BKS, Dayyani I, Friswell MI (2015) Fluid/structure-interaction analysis of the fish-bone-active-camber morphing concept. J Aircr 52(1):307–319
27. Rivero AE, Cooper JE, Woods BKS (2020) Numerically efficient three-dimensional fluid-structure interaction routine for composite camber morphing aerostructures. In: AIAA SciTech 2020 Forum, p 1298

28. Zhang J, Shaw AD, Wang C et al (2021) Aeroelastic model and analysis of an active camber morphing wing. Aerosp Sci Technol 111:106534
29. van Zyl LH, Maserumule MS (2001) Unrestrained aeroelastic divergence and the pk flutter equation. J Aircr 38(3):588–590
30. Rodden WP (1981) Aeroelastic divergence of unrestrained vehicles. J Aircr 18(12):1072–1073
31. Kalman TP, Rodden WP, Giesing JP (1971) Application of the doublet-lattice method to non-planar configurations in subsonic flow. J Aircr 8(6):406–413
32. Bisplinghoff RL, Ashley H (2013) Principles of aeroelasticity. Courier Corporation
33. Chen S, Tang S, Yan H et al (1989) Dynamic stability and active control of elastic vehicles acting with unsteady aerodynamic forces. In: Guidance, navigation and control conference, p 3557